

Preparation, scale-up and application of meso-ZSM-5 zeolite by sequential desilication–dealumination

Hongman Sun^{1,2} · Peng Peng¹ · Youhe Wang^{1,2} · Chencan Li^{1,2} · Fazle Subhan^{1,3} · Peng Bai¹ · Wei Xing^{1,2} · Zhongdong Zhang⁴ · Zhaoyong Liu⁴ · Zifeng Yan¹

Published online: 27 February 2017
© Springer Science+Business Media New York 2017

Abstract Meso-ZSM-5 zeolites with unique catalytic cracking properties have been prepared from commercial ZSM-5 using sequential desilication–dealumination strategy. Desilication and dealumination conditions, including concentration, temperature, dissolution time and liquid–solid ratio were systematically studied and optimized. Characterization results revealed that mesoporosity can be effectively introduced into commercial ZSM-5 crystals by desilication. The introduction of mesopores enables the well interconnectivity of micropores. Concomitant dealumination by removing Al-rich debris from desilicated samples shows superiority in micro- and mesopore network, remedying the limitation of desilication. The removal of the debris preserves intrinsic microporosity and improves the acid site accessibility in zeolites. Based on optimized parameters of porosity tuning tests at 0.25 L scale, the preparation route was scaled up to a pilot scale (50 L). In the heavy oil catalytic cracking test, compared with P-ZSM-5-contained catalyst, A-ZSM-5-contained and ACP-ZSM-5-contained FCC catalyst display increased

heavy oil conversion (from 67.68 to 68.25 and 68.33 wt%, respectively), improved light olefin yield including propylene (from 5.67 to 5.87 and 6.11 wt%, respectively) and promoted yields of both gasoline and diesel.

Keywords Sequential desilication–dealumination · Meso-ZSM-5 zeolites · Catalytic cracking performance · Pilot scale

1 Introduction

With the rapid development of human society, the gap between supply and demand of propylene and other light olefins is greatly increasing. On the other hand, the increased output of heavy oil throughout the world requires to be consumed economically. Converting heavy oil into propylene and other value-added chemicals via catalytic cracking is a promising strategy to achieve such goal. ZSM-5 zeolite, as one of the most important high-silica zeolites, is commonly utilized in catalytic cracking owing to their superior physico-chemical properties such as adjustable acidity, excellent hydrothermal stability and shape-selectivity features [1–3]. However, poor intracrystalline diffusion of large molecules within ZSM-5 pores always results in relatively easy coke formation and accelerates catalyst deactivation, which limits its practical application [4, 5]. Thus, it is still a challenge to further improve propylene selectivity and catalytic lifetime over this catalyst [6].

Shortening the diffusion path and enhancing the accessibility of the micropores via mesopores introduction are crucial and effective approaches to facilitate the catalytic reactions [7]. Tremendous works have been carried out to acquire meso-ZSM-5 by introducing substantial intra- or

✉ Youhe Wang
yhewang@upc.edu.cn

✉ Zifeng Yan
zfyancat@upc.edu.cn

¹ State Key Laboratory for Heavy Oil Processing, CNPC Key Laboratory of Catalysis, China University of Petroleum, Qingdao 266580, China

² College of Science, China University of Petroleum (East China), Qingdao 266580, China

³ Department of Chemistry, Abdul Wali Khan University Mardan, Mardan, K.P.K, Pakistan

⁴ Lanzhou Petrochemical Research Center, China National Petroleum Corporation, Lanzhou 730060, China

intercrystalline mesoporous besides the microporous structure [8]. In recent years, hard template methods (*e.g.* carbon particles [9], carbon aerogel [10] and carbon nanotube [11]) and soft template methods (*e.g.* cetyltrimethylammonium bromide [12], polyethylene oxide-polypropylene oxide-polyethylene oxide-copolymer [13] and organosilane agents [14]) are developed to synthesize the meso-ZSM-5. Although, most of these constructive methods successfully acquire mesoporosity and improve performance in catalytic reactions, both production costs and environmental issues require further evaluation for industrialization. In addition, the main drawback of constructive methods is substantial usage of templates, which can greatly increase the industrialization cost of such materials [15].

In contrast, the destructive methods, including desilication and dealumination, are relatively easier to be implemented on industrial scale [16–18]. Such strategies are directly based on the acidic properties via Brønsted acidity depletion [19]. Yan et al. reported the modification of USY zeolites using multi-hydroxyl carboxylic acid and phosphate, and indicated that dealumination is a promising technique for low-silica Y zeolites modification [20]. However, dealumination may also result in Al-rich debris to form Lewis acid sites which may cause coke formation and thus accelerate the deactivation of catalyst. In addition, the mesopores created by dealumination are poorly interconnected and difficult to control. Furthermore, the dealumination process is restricted to aluminium-rich zeolites [21]. As for the low-aluminum ZSM-5 zeolite, the introduction of mesopores by the alkaline-mediated leaching of framework Si has been deemed more promising due to operational ease and efficiency for the generation of hierarchical structure [22].

The pioneer work by Matsukata and co-workers witnessed the utilization of desilication to optimize the pore structure of ZSM-5 [23]. Recently, several studies have investigated the preparation of meso-zeolites using aqueous NaOH solution. Excellent performance for a wide range of catalytic reactions was achieved including isomerization [24], alkylation [25], acylation [26], aromatization [27] and cracking [28], etc. Desilication could introduce interconnected mesopores and promote the accessibility of internal surface of the zeolite crystal, exhibiting an outstanding advantage for access-limited and diffusion-constrained reactions [29, 30]. However, one of the disadvantages of such process is the creation of non-framework aluminum, which blocks the voids and channels. Maria Milina et al. investigated the mesopore formation and acidity modification in ZSM-5 zeolites via sequential desilication–dealumination [31]. Desilication in alkaline solution leads to abundant mesopores development and dealumination via acid treatment exhibits higher catalytic activities due to textural enhancements by removing aluminium-rich amorphous

debris. However, their experiment was conducted at a bench scale and there still exists a huge challenge on an industrial scale for sequential desilication–dealumination. For example, under the real industrial conditions, it is difficult to avoid the temperature and concentration gradients which will result in a great gap between actual synthesis parameters and required synthesis conditions [32].

Therefore, in this work, we systematically investigated the synthesis parameters for sequential desilication–dealumination of meso-ZSM-5. Besides, the preparation and catalytic cracking performance of meso-ZSM-5 zeolite was scaled up from laboratory to pilot scale (50 L). The results manifest that sequential desilication–dealumination can effectively introduce intracrystalline mesoporosity with high diffusivity, improve the acid site accessibility in zeolites through desilication in alkaline medium and remove the non-framework aluminum in dilute acid medium. Meso-ZSM-5, as FCC additives, can improve the yield of propylene and light olefins, and promote the heavy oil conversion rate and the yield of light end products (gasoline and diesel).

2 Experimental sections

Meso-ZSM-5 was prepared by a two-step strategy, as depicted in Fig. 1. First, commercial ZSM-5 (parent material) was treated by aqueous NaOH solution to introduce mesopore into ZSM-5 structure. Then, acid treatment using HCl solution was conducted to remove the non-framework aluminum and open up the micropore path to further enhance the accessibility inside the pores.

2.1 Preparation of meso-ZSM-5 at 0.25 L scale

Meso-ZSM-5 zeolite was prepared from commercial ZSM-5 zeolite by sequential desilication–dealumination strategy. The parent zeolite is H-form ZSM-5 with $\text{SiO}_2/\text{Al}_2\text{O}_3$ mole ratio of 27.4 (obtained from Zibo Catalyst Company). In a typical synthesis, 5 g ZSM-5 zeolite and 150 mL of 0.4 mol L^{-1} aqueous NaOH solution were mixed by vigorous stirring at 353 K for 60 min. Then the product was collected by filtration followed by washing with deionized water and drying at 383 K overnight. The alkali-treated sample was transferred into 0.1 mol L^{-1} HCl aqueous solution (5 g zeolite per 50 mL of solution) and reacted for 5 h at 353 K, followed by filtration, washing with deionized water and finally dried at 338 K overnight.

2.2 Preparation of meso-ZSM-5 zeolite at 50 L scale

Based on the preparation of meso-ZSM-5 at 0.25 L scale, the synthesis process was scaled-up to pilot scale (50 L).

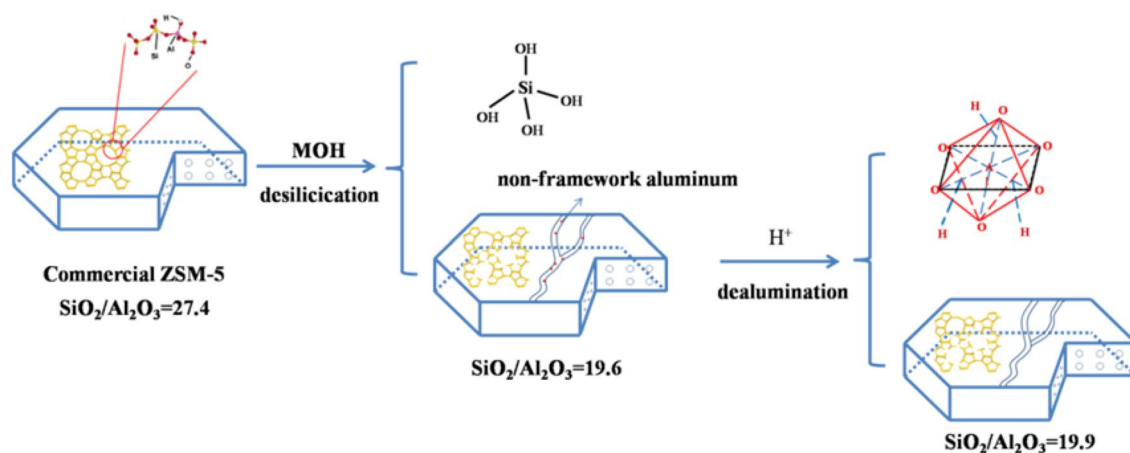


Fig. 1 Schematic representation of sequential desilication–dealumination

The preparation reactor was manufactured by Weihai Xintai Chemical Equipment Co. Ltd. For pilot scale preparation, 1000 g ZSM-5 zeolite and 30 L of 0.4 mol L⁻¹ NaOH solution was first mixed by vigorous stirring at 353 K for 60 min. Then, the product was collected by filtration, followed by washing with deionized water and drying at 383 K overnight. The alkali-treated sample was transferred into 0.1 mol L⁻¹ HCl aqueous solution (1000 g zeolite per 10 L of solution) and reacted for 5 h at 353 K, followed by filtration, washing with deionized water and then dried at 338 K overnight. The samples obtained after sequential desilication–dealumination strategy were denoted as A-ZSM-5 and ACP-ZSM-5, respectively. In order to study their acidity and catalytic performance, A-ZSM-5 and ACP-ZSM-5 samples were converted into ammonium form via three consecutive ion-exchanges in 0.5 mol L⁻¹ NH₄Cl aqueous solution and finally calcined at 823 K for 4 h. In addition, the raw material was referred as P-ZSM-5.

2.3 Characterization

Phase analysis was performed on X-ray diffractometer (PAN analytical X'Pert PRO MPD) with Cu K α radiation. Relative crystallinity (R.C.) was calculated by taking the ratio of peak area (22.5–25°) of meso-ZSM-5 and parent ZSM-5 at the same 2 θ range [33]. Nitrogen adsorption–desorption isotherms were measured using Micrometrics Tristar 3000 (0.25 L) and ASAP 2000 (50 L) analyzer at 77 K. Barrett-Emmett-Teller (BET) surface area was measured using the adsorption branch data in the relative pressure (P/P₀) range from 0.06 to 0.2 [34], and the micropore volume (V_{micro}) was calculated by the t-plot method [35]. The pore size distribution was calculated by BJH method using nitrogen adsorption branch data. To further investigate the relative variation in micro- and

mesoporosity, the indexed hierarchical factor (IHF) was calculated by the following equation [29]:

$$IHF = \frac{S_{meso}}{S_{meso,max}} \times \frac{V_{micro}}{V_{micro,max}} \quad (1)$$

where $S_{meso,max}$ and $V_{micro,max}$ are the largest value of S_{meso} and V_{micro} among the as-prepared samples.

Morphologies of all samples were investigated using scanning electron microscopy (SEM, Hitachi S4800) and transmission electron microscopy (TEM, JEOL JEM2100UHR). Temperature-programmed desorption of ammonia (NH₃-TPD) was investigated in a CHEMBET 3000 TPR/TPD equipment. 200 mg of samples was pretreated at 773 K in He flow (120 cm³ min⁻¹) for 1 h. Afterwards, NH₃ (120 cm³ min⁻¹) was adsorbed at 353 K for 40 min followed by He purging at the same temperature for 1 h. Desorption of NH₃ was monitored in the temperature range of 353–1073 K at a ramp rate of 10 K min⁻¹. Pyridine adsorbed Fourier transform infrared spectroscopy (Py-FTIR) was measured at a Thermo Nicolet NEXUS spectrometer. Before analysis, each sample was dried at 573 K for 3 h. In order to reach equilibrium, the adsorption of pyridine was conducted at room temperature for 24 h. Then the samples were evacuated at 423 K for 3 h to remove physisorbed species. Collidine adsorbed Fourier transform infrared spectroscopy (Coll-FTIR) was collected using the similar method as that of Py-FTIR. “Accessibility index” (ACI) is introduced to quantify the accessibility of acid sites available to larger molecules, which is calculated by using following equation [36]:

$$ACI = \frac{C_{BC}}{C_{whole}} \approx \frac{C_{BC}}{C_{BP}} \quad (2)$$

where C_{BC} is the amount of Brønsted acid sites from Coll-FTIR; C_{whole} is the amount of Brønsted acid sites from Py-FTIR, which approximately equals C_{BP} .

The Si/Al ratios of samples was measured by wavelength dispersive X-Ray fluorescence spectrometer produced by PANalytical B.V. ^{27}Al solid state Magic angle spinning nuclear magnetic resonance (^{27}Al MAS NMR) spectra were recorded with a frequency of 104.18 MHz, a spinning rate of 10.0 kHz, and a recycling delay of 4 s.

2.4 Catalyst preparation and catalytic evaluation tests

The FCC catalysts were prepared as follows: pseudo-boehmite (Shandong aluminum plant), alumina sol (Lanzhou petrochemical company), kaolin (Suzhou), USY (Lanzhou petrochemical company), H form ZSM-5 and deionized water were mixed at a mass ratio of 20:6:30:32:12:80. After sprayed molding, the products were calcined at 773 K for 50 min. Then, pre-deactivation by hydrothermal treatment of fresh catalyst was conducted at 1073 K for 10 h.

The FCC performance was tested in a fixed fluidized bed microactivity test under typical FCC microactive testing conditions. Each FCC test was repeated three times for accuracy and the present reaction result is an average of three parallel tests. The reaction temperature was 773 K, reaction time was 60 s, and catalyst-to-oil mass ratio was 4.0. Properties of Lanzhou vacuum gas oil (VGO) feedstock are listed in Table 1. The components of the cracking gas including dry gas and liquefied petroleum gas were detected by a Varian 3800C gas chromatography. The content of liquid products (gasoline, diesel and heavy cycle oil (HCO)) was determined by Agilent 7890 A gas chromatograph. Coke yield was analysed by elemental analyzer (Elementar Vario EL III). Moreover, the conversion and yield during the FCC reactions were calculated by following equation [37]:

$$\text{Yield of product } i = \frac{\text{mass of product } i}{\text{total mass in the feed}} \times 100\% \quad (3)$$

$$\text{Conversion} = 100\% - \text{yield of HCO} - \text{yield of diesel} \quad (4)$$

Table 1 Properties of vacuum gas oil (VGO) feedstock used in the FCC experiments

Properties	Element	Value
Density at 293 K (kg m^{-3})		879.1
Residual coke (wt%)		4.31
Elemental analysis ($\mu\text{g g}^{-1}$)	C	86.18
	H	12.57
	S	0.46
	N	0.30
Metal content (wt%)	V	6.57
	Ni	4.42
Group composition (wt%)	Saturates	56.2
	Aromatics	38.3
	Resin and asphaltene	5.5

$$\text{Yield of light oil} = \text{yield of gasoline} + \text{yield of diesel} \quad (5)$$

$$\text{Yield of total liquid oil} = \text{yield of light oil} + \text{yield of liquefied petroleum gas} \quad (6)$$

3 Results and discussion

3.1 Process controlling at 0.25 L scale during desilication

3.1.1 Effects of $\text{OH}^-/\text{ZSM-5}$ ratio

$\text{OH}^-/\text{ZSM-5}$ (or $\text{H}^+/\text{ZSM-5}$) ratio represents the volume of alkali (or acid) aqueous solution to parent ZSM-5 zeolites by weight and it has a direct impact on the production of meso-ZSM-5 zeolites at an industrial scale. In this set of experiments, the effect of $\text{OH}^-/\text{ZSM-5}$ ratios in the range of 10, 20, 30 and 40 mL g^{-1} was also investigated (Fig. 2). Temperature, time and NaOH concentration were kept at 353 K, 60 min and 0.4 mol L^{-1} , respectively.

As can be seen in Fig. 2a, with the increase of $\text{OH}^-/\text{ZSM-5}$ ratio, the relative crystallinity exhibits a sharp decrease possibly due to skeleton damage caused by desilication process. The relative crystallinity reached at 72% when $\text{OH}^-/\text{ZSM-5}$ ratio is 40 mL g^{-1} . Although alkali treatment can damage the skeleton of the zeolites, the retention of five characteristic peaks at 2θ of 22.5 to 25° indicates the structure did not collapse completely.

Nitrogen adsorption–desorption isotherms of samples 1–5 are shown in Fig. 2b. The commercial zeolites (sample 1) displays a type I adsorption isotherm. After desilication, all the four samples show an obvious H4 hysteresis loops after relative pressure (P/P_0) of 0.42, which means the formation of mesopores. However, when $\text{OH}^-/\text{ZSM-5}$ ratio is 40 mL g^{-1} , the N_2 quantity absorbed is much lower than sample 1 due to alkali aqueous solution severely damaged the skeleton of zeolites and reducing the number of micropores. As for $\text{OH}^-/\text{ZSM-5}$ ratio are 10 and 20 mL g^{-1} , even though the samples have a higher relative crystallinity, the majority of its pores is smaller than sample 2. Thus, optimal $\text{OH}^-/\text{ZSM-5}$ ratio of 30 mL g^{-1} was selected for further experiments.

3.1.2 Effects of temperature

Desilication temperature is another key parameter for ZSM-5 zeolites. In this series of experiments, the influence of temperature during desilication in the temperature range of 313–368 K has been investigated using a 0.4 mol L^{-1} NaOH solution as alkaline medium, $\text{OH}^-/\text{ZSM-5}$ ratio of 30 mL g^{-1} and 60 min of dissolution time.

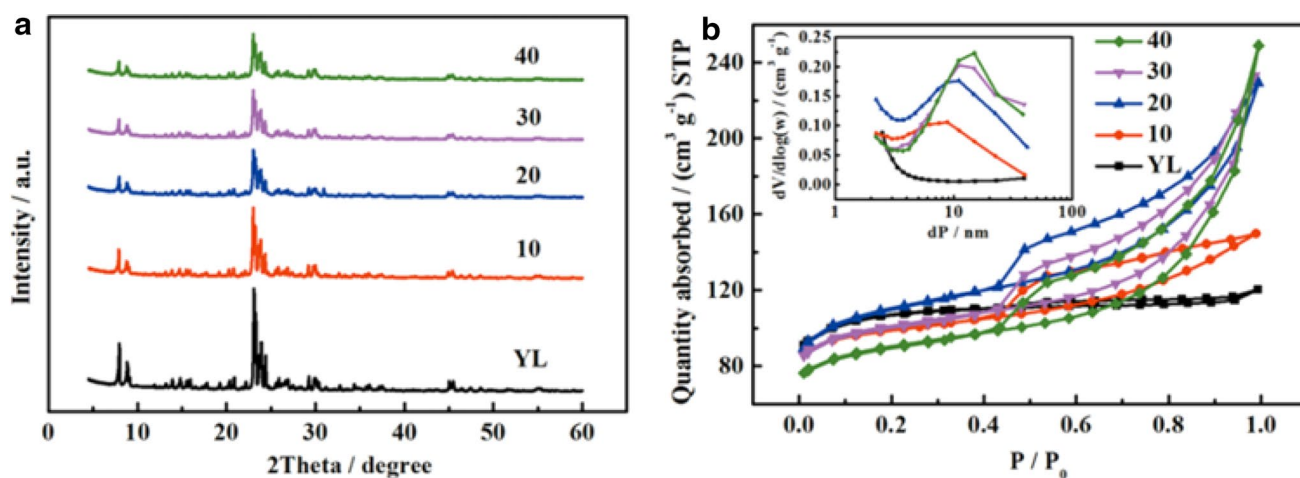


Fig. 2 XRD patterns (a), nitrogen adsorption desorption isotherms (b) and pore size distribution (*inset*) of parent ZSM-5 (sample 1), meso-ZSM-5 with OH⁻/ZSM-5 ratio of 30 mL g⁻¹ (sample 2), 10 mL g⁻¹ (sample 3), 20 mL g⁻¹ (sample 4), 40 mL g⁻¹ (sample 5)

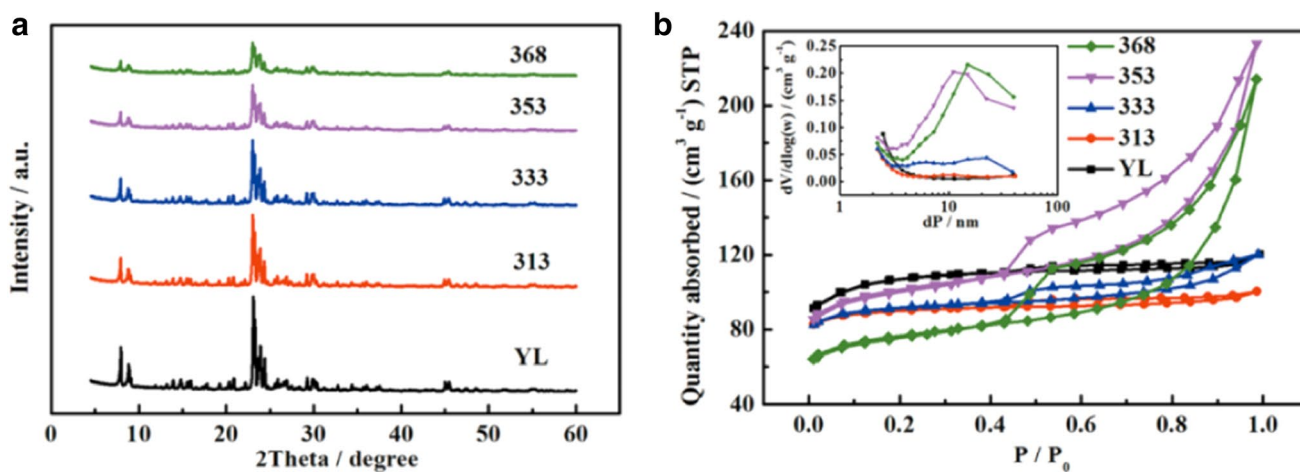


Fig. 3 XRD patterns (a), nitrogen adsorption desorption isotherms (b) and pore size distribution (*inset*) of parent ZSM-5 (sample 1), meso-ZSM-5 with OH⁻/ZSM-5 ratio of 353 K (sample 2), 313 K (sample 6), 333 K (sample 7), 368 K (sample 8)

Desilication temperature strongly affected the relative crystallinity of meso-ZSM-5 (Fig. 3a). When the desilication temperatures were 313, 333 and 353 K, the relative crystallinity can maintain 70%. With further increase in desilication temperature to 368 K, the relative crystallinity has a sharp decrease to 64%, revealing that the skeleton of zeolites had been changed severely and the structure collapsed at a certain degree.

Moreover, from nitrogen adsorption–desorption isotherms in Fig. 3b, the absorbed N₂ quantity of sample 8 is much lower than sample 1. It also infers that higher desilication temperatures at 368 K caused collapse of zeolites. In the cases of lower desilication temperatures from 313 to 333 K, pore size distribution (Fig. 3b) focused below

10 nm. This result demonstrates the lower desilication temperatures are unable to generate sufficient mesoporosity. Thus, optimal desilication temperature was 353 K.

3.1.3 Effects of time

In addition to temperature, dissolution time can directly affect the relative crystallinity and textural properties. In this set of experiments, dissolution time was varied to 30, 60, 90 and 120 min. The other parameters were identical to the standard protocol.

As shown in Fig. 4a, even if dissolution time was carried on 30 min, the relative crystallinity has a sharp decrease. This indicates that the rate of alkali dissolution is so fast

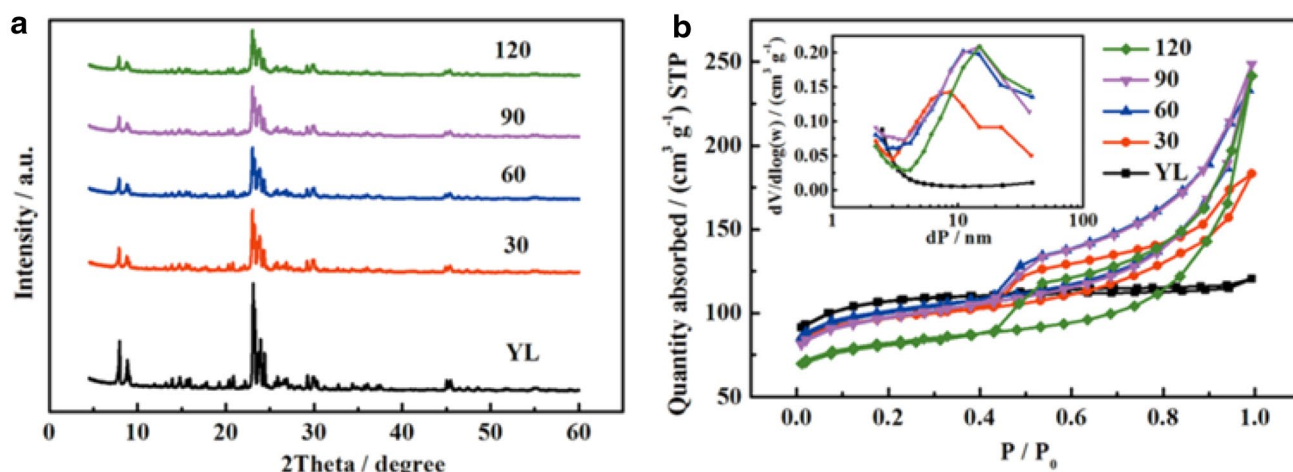


Fig. 4 XRD patterns (a), nitrogen adsorption-desorption isotherms (b) and pore size distribution (*inset*) of parent ZSM-5 (sample 1), meso-ZSM-5 with time of 60 min (sample 2), 30 min (sample 9), 90 min (sample 10), 120 min (sample 11)

that it can damage the skeleton of zeolites within 30 min. However, the V_{meso} of sample 9 is smallest, which is not big enough to facilitate the diffusion effect. When alkali dissolution reaches 120 min, the S_{BET} is lowest indicating that a long dissolution time will destroy the micropores excessively. When dissolution time was selected as 60 and 90 min, the relative crystallinity and textural properties were similar. Considering the relatively higher cost at 90 min, optimal dissolution time of 60 min was fixed for further experiments.

3.1.4 Effects of NaOH concentration

NaOH concentration is one of the pivotal factors affecting the cost of the zeolite production. The influence of NaOH

concentration in the range of 0.2–0.5 mol L⁻¹ is conducted similar to that of other experimental parameters keeping temperature at 353 K, OH⁻/ZSM-5 ratio of 30 mL g⁻¹ and time of 60 min. As shown in Fig. 5a, the relative crystallinity decreases with the increase of NaOH concentration. When the NaOH concentration is up to 0.5 mol L⁻¹, the relative crystallinity is only 69% which means immoderate dissolution of the ZSM-5 skeleton. This phenomenon is corresponding with its lowest absorbed N₂ quantity and biggest pore distribution. However, when the NaOH concentration is 0.2 and 0.3 mol L⁻¹, the V_{meso} is 0.1202 and 0.1788 cm³/g, respectively, which represents insufficient desilication. Therefore, the optimal NaOH concentration was 0.4 mol L⁻¹.

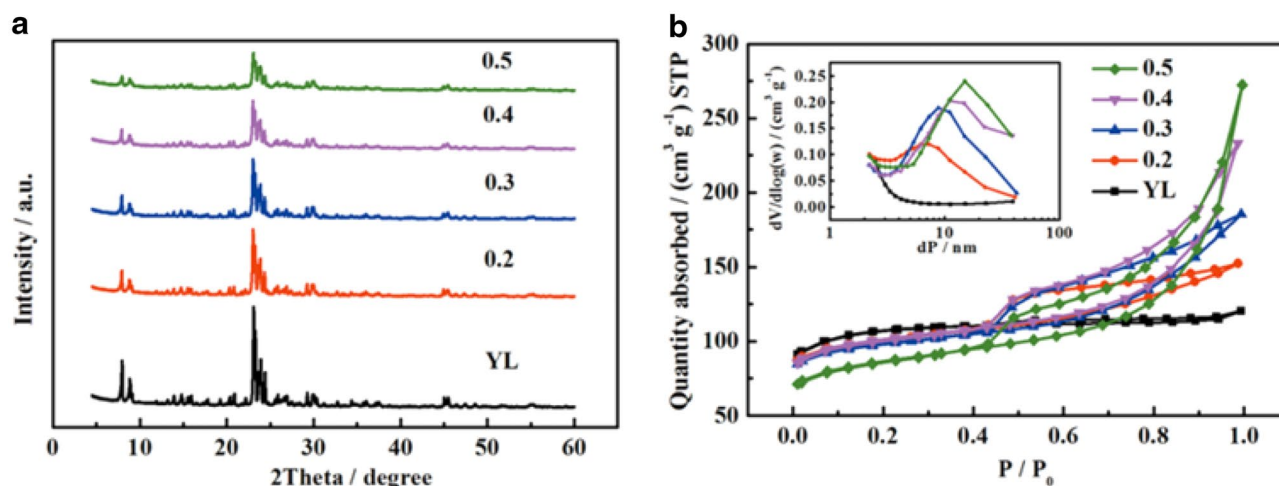


Fig. 5 XRD patterns (a), nitrogen adsorption-desorption isotherms (b) and pore size distribution (*inset*) of parent ZSM-5 (sample 1), meso-ZSM-5 with NaOH concentration of 0.4 mol g⁻¹ (sample 2), 0.2 mol g⁻¹ (sample 12), 0.3 mol g⁻¹ (sample 13), 0.5 mol g⁻¹ (sample 14)

Table 2 Textural properties of meso-ZSM-5 prepared at 0.25 L scale

No.	Class	$S_{BET}/m^2\ g^{-1}$	$V_{BJH}/cm^3\ g^{-1}$	Note
1	ZSM-5	332	0.0341	Parent zeolite
2	Standard synthesis protocol	317	0.2516	$OH^-/ZSM-5$ ratio is kept at 30 mL g^{-1} temperature is kept at 353 K dissolution time is kept at 60 min NaOH concentration is kept at 0.4 mol g^{-1}
3	Effects of $OH^-/ZSM-5$ ratio	308	0.1148	$OH^-/ZSM-5$ ratio is kept at 10 mL g^{-1}
4		311	0.2444	$OH^-/ZSM-5$ ratio is kept at 20 mL g^{-1}
5		294	0.2948	$OH^-/ZSM-5$ ratio is kept at 40 mL g^{-1}
6	Effects of temperature	274	0.0280	Temperature is kept at 313 K
7		280	0.0627	Temperature is kept at 333 K
8		241	0.2531	Temperature is kept at 368 K
9	Effects of time	303	0.1716	Time is kept at 30 min
10		308	0.2866	Time is kept at 90 min
11		258	0.2874	Time is kept at 120 min
12	Effects of NaOH concentration	315	0.1202	NaOH concentration is kept at 0.2 mol g^{-1}
13		307	0.1788	NaOH concentration is kept at 0.3 mol g^{-1}
14		275	0.3434	NaOH concentration is kept at 0.5 mol g^{-1}

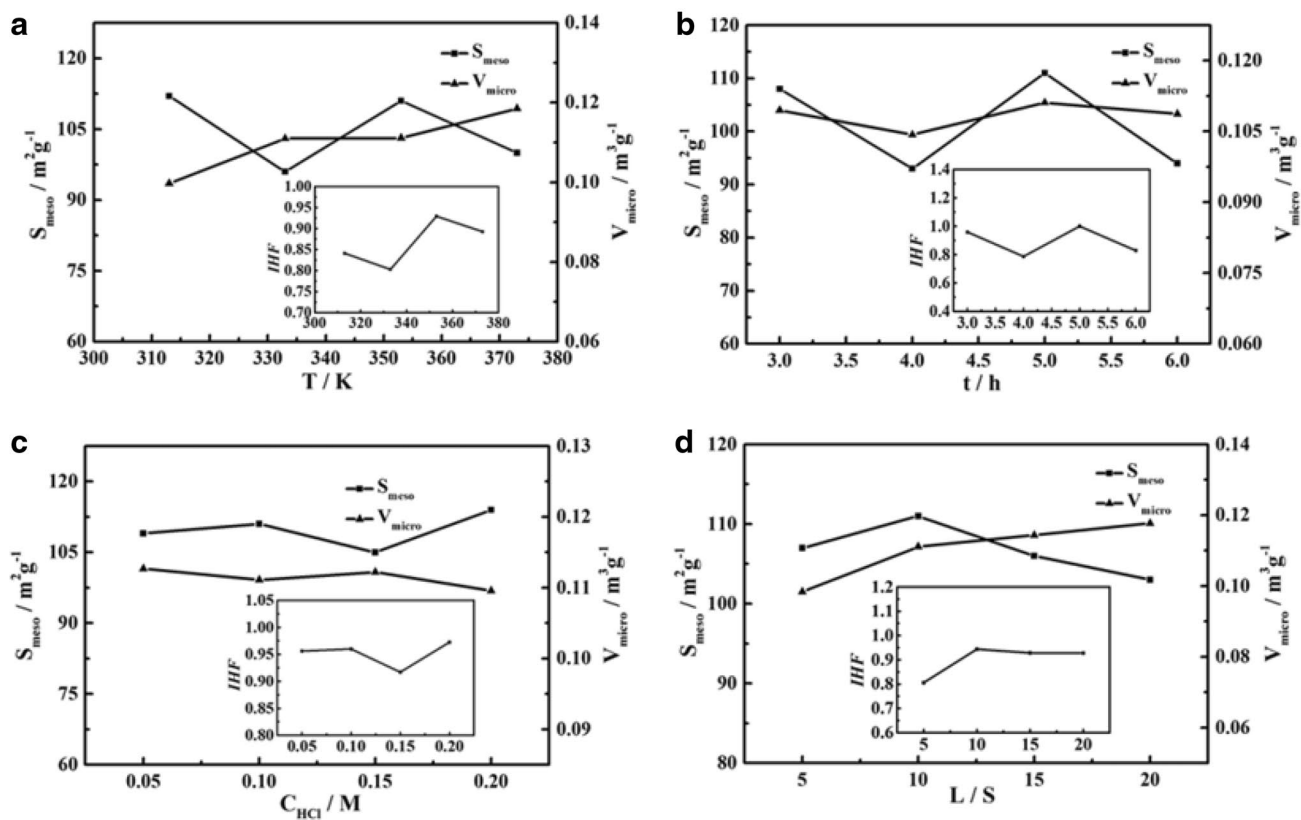


Fig. 6 The influence of temperature (a), dissolution time (b), HCl concentration (c) and $H^+/ZSM-5$ ratio (d) on the S_{meso} , V_{micro} , and IHF (inset)

Thus, from the above discussion and textural properties shown in Table 2, the optimal condition of desilication is described as follows: 5 g ZSM-5 zeolite was first mixed with 150 mL NaOH solution (0.4 mol L^{-1}). After vigorous

stirring at 353 K for 60 min, the products were collected by filtration followed by washing with deionized water, and dried at 383 K overnight.

3.2 Porosity tuning at 0.25 L scale during subsequent dealumination

Based on the optimal products of desilication, preparation parameters during subsequent dealumination were investigated as follows. The percentage of relative crystallinity and *IHF* were combined to analyze the optimal condition of subsequent dealumination.

3.2.1 Effects of temperature

The effect of temperature in the range of 313–368 K was investigated over dealumination as shown in Fig. 6a keeping dissolution time, $H^+/ZSM-5$ ratio and HCl concentration to 5 h, 10 mL g^{-1} and 0.1 mol L^{-1} , respectively. As shown, when the temperature was 353 K, the *IHF* was maximized to 0.93. Thus, optimal temperature of 353 K was selected.

3.2.2 Effects of alkali dissolution time

The effect of dissolution time in the range of 3–6 h is shown in Fig. 6b. Such analysis was performed using temperature at 353 K, $H^+/ZSM-5$ ratio of 10 mL g^{-1} and HCl concentration of 0.1 mol L^{-1} . As can be seen from Fig. 6b, when the dissolution time was 5 h, *IHF* was maximized to 1.00. Thus, the optimal dissolution time was 5 h.

3.2.3 Effects of $H^+/ZSM-5$ ratio

The effect of HCl concentration is shown in Fig. 6c. Temperature, time and $H^+/ZSM-5$ ratio was kept at 353 K, 5 h and 10 mL g^{-1} , respectively. From Fig. 6c, we can see that when HCl concentration was 0.1 mol L^{-1} , the *IHF* was maximized to 0.96. Thus, the optimal concentration of 0.1 mol L^{-1} was selected for dealumination.

3.2.4 Effects of NaOH concentration

The effect of $H^+/ZSM-5$ ratios is shown in Fig. 6d while keeping temperature, dissolution time and HCl concentration at 353 K, 5 h and 0.1 mol L^{-1} , respectively. When the $H^+/ZSM-5$ ratio was 10 mL g^{-1} , *IHF* was maximized to 0.94. Thus, an optimal $H^+/ZSM-5$ ratio was 10 mL g^{-1} .

From the above discussion, the optimal condition of subsequent dealumination is described as follows: The alkali-treated sample was transferred into 0.1 mol L^{-1} HCl aqueous solution (5 g zeolite per 50 ml of solution) and reacted for 5 h at 353 K, followed by filtration, washing with deionized water and then dried at 338 K overnight.

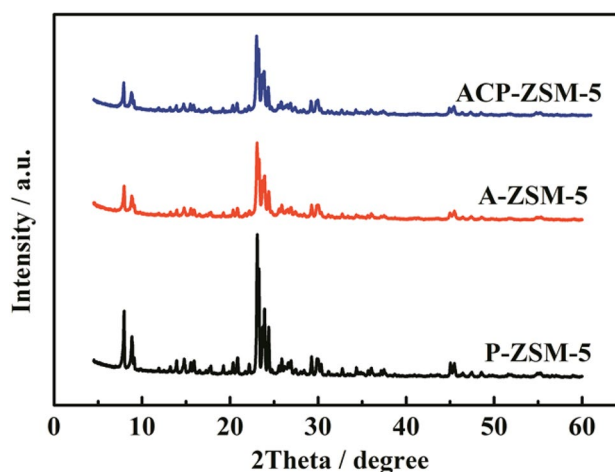


Fig. 7 XRD patterns of P-ZSM-5, A-ZSM-5 and ACP-ZSM-5

3.3 Scale up

From the results of single-factor experiment described in Sect. 3.1, desilication played a vital role in constructing mesoporous structures of ZSM-5-based zeolites. Subsequent dealumination promoted the maturity of micro- and mesopore texture and manifested its crucial influence on relative crystallinity. Thus, the preparation process was scaled-up to pilot scale (50 L) based on the optimized conditions and further investigated the relationship between structure, acidity, and FCC catalytic application of meso-ZSM-5 zeolite by sequential desilication–dealumination.

3.3.1 XRD analysis

The XRD patterns of meso-ZSM-5 after sequential desilication–dealumination are shown in Fig. 7. A-ZSM-5 and ACP-ZSM-5 samples exhibit two diffraction peaks at $2\theta=7$ to 8° and five characteristic peaks at $2\theta=22.5$ to 25° , indicating the characteristic peaks of zeolite. As shown in Table 3, compared to the case of P-ZSM-5 sample, A-ZSM-5 shows a sharp decrease of relative crystallinity and SiO_2/Al_2O_3 ratio, which is caused by desilication in alkaline medium. However, ACP-ZSM-5 exhibited a mild increase of relative crystallinity and SiO_2/Al_2O_3 ratio, because the acid processing will remove the non-framework aluminium instead of damaging the skeleton of ZSM-5. Obviously, sequential desilication–dealumination possesses superiority in preserving the inherent acidity and perfecting the pore structure.

3.3.2 Textural properties

The detailed textural characteristics of the obtained meso-ZSM-5 samples were illustrated by nitrogen

Table 3 Textural properties and relative crystallinities of meso-ZSM-5 prepared at 50 L scale

Samples	SAR ^a	R.C. ^b (%)	S _{BET} ^c (m ² g ⁻¹)	S _{micro} ^d (m ² g ⁻¹)	S _{meso} ^e (m ² g ⁻¹)	V _{total} ^f (cm ³ g ⁻¹)	V _{micro} ^g (cm ³ g ⁻¹)	V _{meso} ^h (cm ³ g ⁻¹)	IHF
P-ZSM-5	27.4	100	241.8	230.9	10.9	0.148	0.123	0.054	0.16
A-ZSM-5	19.6	78	304.6	252.4	52.2	0.374	0.131	0.265	0.81
ACP-ZSM-5	19.9	82	317.9	254.1	63.8	0.386	0.133	0.276	1.00

^aCalculated by XRF. SAR represents SiO₂/Al₂O₃ mole ratio

^bCalculated by XRD. R.C. represents the relative crystallinity

^cBET surface areas

^dMicropore surface areas calculated by t-plot method

^eMesopore surface areas equal to S_{BET} minus S_{micro}

^fTotal pore volume measured at a relative pressure (P/P₀) of 0.99

^gThe t-plot micropore volume

^hBJH adsorption cumulative volume

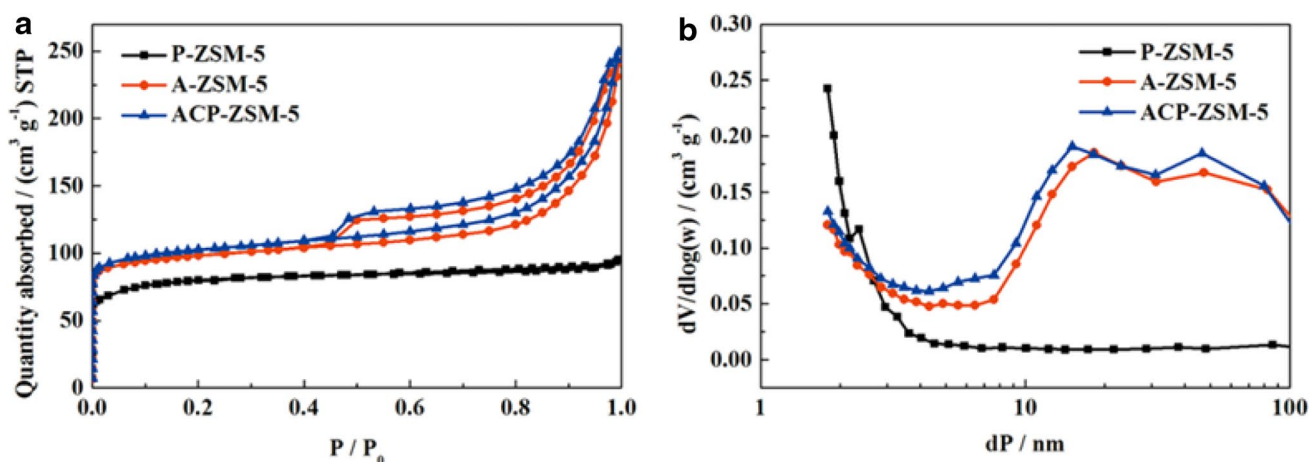


Fig. 8 Nitrogen adsorption–desorption isotherms (a) and pore size distribution calculated from the BJH adsorption branch (b)

adsorption–desorption isotherms at 77 K. As shown in Fig. 8a, the P-ZSM-5 sample shows a type I adsorption isotherm, revealing the microporous nature. For A-ZSM-5 and ACP-ZSM-5, the isotherm change to type IV with a significant H4 hysteresis loops after relative pressure (P/P₀) of 0.42, indicating the formation of mesopores. The BJH pore size distribution (Fig. 8b) proves the formation of abundant mesopores after desilication and subsequent dealumination, attributing to the degradation of the ZSM-5 framework [19]. The textural properties summarized in Table 3 also revealed that the mesopore surface area and pore volume of ACP-ZSM-5 increases compared with those of A-ZSM-5 due to the fact that acid wash can remove the non-framework aluminium in pore mouths and open up the pore channels. Thus, the dealumination process significantly improves the mesoporosity of zeolites. The formation of the developed mesopores and unobstructed pore mouths could facilitate catalytic cracking performance to a great extent [22].

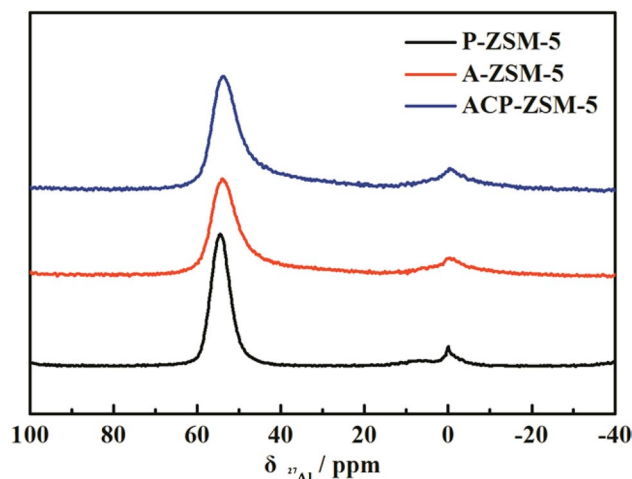


Fig. 9 ²⁷Al MAS NMR spectra of P-ZSM-5, A-ZSM-5 and ACP-ZSM-5

3.3.3 ^{27}Al MAS NMR tests

The influence of post treatments on the coordination of aluminum in the zeolite was investigated by ^{27}Al MAS NMR measurement. As shown in Fig. 9, each spectrum exhibits a sharp signal at 55 ppm, which is attributed to the aluminum species with a tetrahedral coordination. In addition, a minor signal at 0 ppm is related to the octahedrally-coordinated Al or non-framework aluminum [38]. Compared with P-ZSM-5, the signal at 55 ppm for A-ZSM-5 obviously decreases; meanwhile the signal at 0 ppm strengthens. ^{27}Al MAS NMR inferred that the desilication lead to the formation of mesopore and generation of octahedrally-coordinated aluminum. For ACP-ZSM-5, the relatively strong signal of tetrahedrally-coordinated aluminum further confirmed the elimination of octahedrally coordinated

aluminum by subsequent dealumination and the generation of pure framework with partially reintegrated Al.

3.3.4 Morphology characterization

Figure 10 shows the morphologies of the as-prepared samples. The P-ZSM-5 possesses rectangular or hexagonal structure with smooth surface (Fig. 10a). Compared with P-ZSM-5, A-ZSM-5 and ACP-ZSM-5 can still maintain their original morphologies due to the post treatments, which slightly affect the external surface of the zeolite crystals (Fig. 10c, e). TEM images of A-ZSM-5 and ACP-ZSM-5 shown in Fig. 10d, f evidenced that the desilication and subsequent dealumination lead to the formation developed mesoporosity in the zeolite framework. Considering

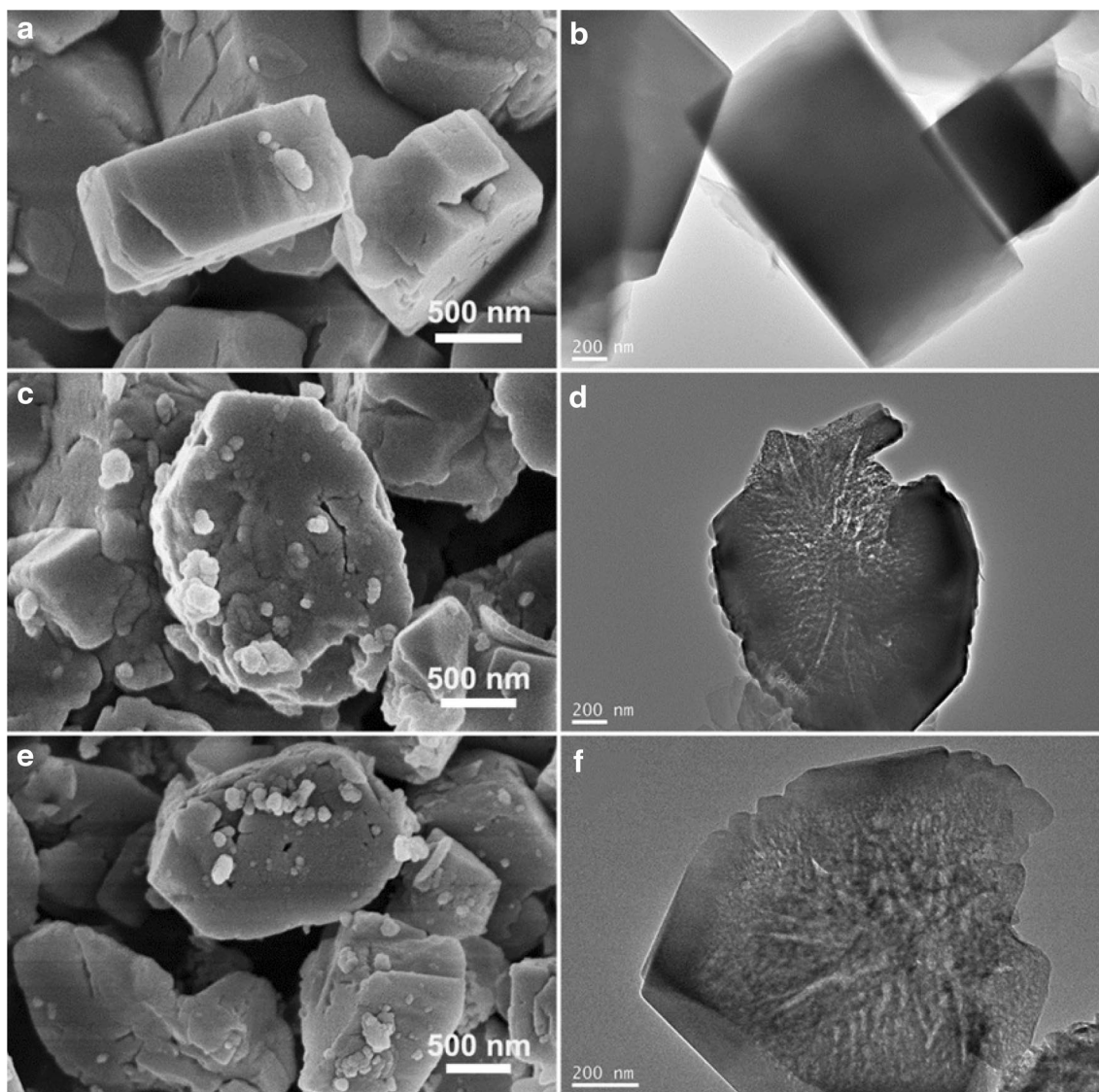


Fig. 10 SEM and corresponding TEM images of P-ZSM-5 (a, b), A-ZSM-5 (c, d) and ACP-ZSM-5 (e, f)

the enhanced textural properties data in Table 3, the structure of intracrystalline mesopore can be confirmed.

3.3.5 Acidic properties

Acidity is also an important property of zeolites for practical applications. In order to investigate acid sites on the surface of all samples, Ammonia temperature-programmed desorption (NH₃-TPD) was collected. As depicted in Fig. 11, the obtained samples display two principal absorbance bands in NH₃ spectrum with NH₃ adsorption at 353 K. The NH₃ desorption maximum centering at 550 K is assigned to weak acid sites, while the high temperature contribution at 780 K is associated with strong acid sites [39]. Compared with parent ZSM-5, the amount of NH₃ adsorbed on weak and strong acid sites decreases for A-ZSM-5, and the tendency is especially strong for acid

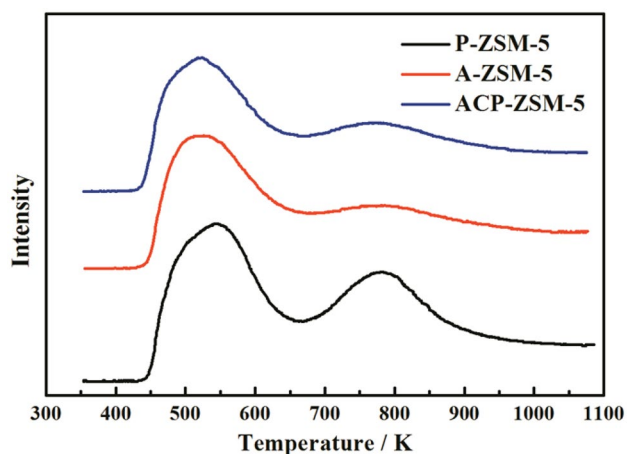


Fig. 11 NH₃-TPD profiles of P-ZSM-5, A-ZSM-5 and ACP-ZSM-5

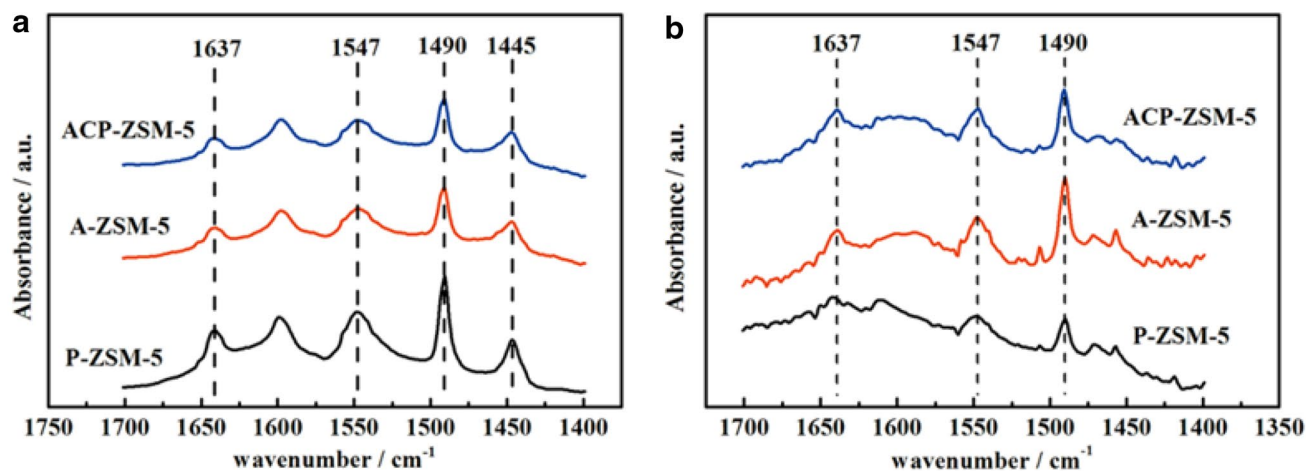


Fig. 12 FTIR spectra of pyridine (a) and collidine adsorption (b) of P-ZSM-5, A-ZSM-5 and ACP-ZSM-5

sites, originating from the destruction of skeleton during desilication. After subsequent dealumination, the amount of weak acid sites falls from 1.341 to 1.293 mmol g⁻¹, and the amount of strong acid sites rises from 0.727 to 0.852 mmol g⁻¹. This is mainly attributed to the removal of the non-framework aluminum in the molecular sieve by subsequent dealumination. NH₃-TPD results, combined with the previous XRF data, reveal that the removal of Al-rich debris by the subsequent dealumination promotes the recovery of the acid properties.

Pyridine adsorbed Fourier transform infrared spectroscopy (Py-FTIR) was further conducted to clarify total acidity into Brønsted and Lewis acid sites and the Py-FTIR profiles are shown in Fig. 12a. Four characteristic bands of pyridine adsorption can be observed. The vibration bands at 1547 and 1637 cm⁻¹ attributed to the adsorption pyridine on Brønsted acid sites, while the bands at 1445 cm⁻¹ correspond to the adsorption on Lewis acid sites. The band at 1490 cm⁻¹ is assigned to adsorption on both Brønsted and Lewis acid sites [40]. The detailed information of acidic properties of P-ZSM-5, A-ZSM-5 and ACP-ZSM-5 are listed in Table 4. Among the textured samples, P-ZSM-5 exhibited a large amount of Brønsted and Lewis acid sites, which is possibly originated from its MFI framework. After desilication, the quantity of Brønsted acid sites exhibits a sharp decrease from 0.538 to 0.297 mmol g⁻¹. The decrease of Brønsted acid is attributed to severe etching of the zeolite skeleton made by the desilication. However, the subsequent dealumination can preserve the total amount of acid sites in zeolite skeleton, which is in good agreement with the XRD results.

To evaluate the accessibility of acid sites, Coll-FTIR test and ACI are introduced in Fig. 12b and Table 4. Seeing the strong steric effect of collidine due to its large molecular diameter of 0.74 nm compared with the 0.54 nm pores in

Table 4 Total acidity, acid distribution and acid site accessibility of meso-ZSM-5 prepared at 50 L scale

Sample	Pyridine adsorbed (mmol g ⁻¹)				Collidine adsorbed (mmol g ⁻¹)	
	C _{BP} ^a	C _{LP} ^b	C _{BP} +C _{LP}	C _{BP} /C _{LP}	C _{BC} ^c	ACI
P-ZSM-5	0.538	0.173	0.711	3.117	0.043	0.079
A-ZSM-5	0.297	0.131	0.428	2.258	0.046	0.156
ACP-ZSM-5	0.257	0.138	0.395	1.856	0.057	0.223

^aC_{BP} represents the amount of pyridine adsorbed on Brønsted acid sites

^bC_{LP} represents the amount of pyridine adsorbed on Lewis acid sites

^cC_{BC} represents the amount of collidine adsorbed on Brønsted acid sites

Table 5 Acidity and acid distribution of meso-ZSM-5 prepared at 50 L scale

Sample	C _w (mmol g ⁻¹)	C _s (mmol g ⁻¹)	C _w +C _s (mmol g ⁻¹)	C _w /C _s
P-ZSM-5	1.533	1.217	2.750	1.260
A-ZSM-5	1.341	0.727	2.068	1.845
ACP-ZSM-5	1.293	0.852	2.145	1.518

C_w represents the amount of NH₃ adsorbed on weaker acid sites. C_s represents the amount of NH₃ adsorbed on strong acid sites

conventional ZSM-5, collidine was used as probe molecule to verify the availability of acid sites in larger pores rather than those in ZSM-5. The P-ZSM-5 shows different absorbance for Coll-FTIR (0.043 mmol g⁻¹) and Py-FTIR (0.538 mmol g⁻¹), and ACI value of 0.079. These parameters indicate that P-ZSM-5 mainly possesses a microporous structure and collidine is mostly adsorbed on their external surface. After desilication, the concentration of Brønsted acid sites detected by Py-FTIR shows a sharp decrease, but the one detected by Coll-FTIR increases. Considering the increase of ACI value from 0.079 to 0.156, these results are due to the formation of intracrystalline mesopore, which is consistent with TEM results. An obvious increase in ACI value (from 0.156 to 0.223) appears after subsequent dealumination, confirming that acid treatment is highly beneficial to unblock pore mouths and hence further increase accessibility (Table 5).

3.3.6 Conversions and product distributions of FCC

Table 6 demonstrates the conversions and product distributions of the FCC catalysts. It is obvious that if desilicated ZSM-5 (i.e. A-ZSM-5) is served as additive for FCC catalyst, both the feedstock conversion and liquefied petroleum gas yield increase from 67.68% and 18.86–68.25% and 18.96%, respectively. Interestingly, A-ZSM-5-contained FCC catalyst shows superior propylene yield (5.87%) compared with the parent ZSM-5-contained catalyst (5.67%). The outstanding performance of meso-ZSM-5 can be

Table 6 Conversions and product distributions of FCC catalysts

Yield of product/wt%	P-ZSM-5	A-ZSM-5	ACP-ZSM-5
Dry gases	2.11	1.91	1.89
Liquefied petroleum gas	18.86	18.96	19.19
Propylene	5.67	5.87	6.11
Gasoline	38.87	39.55	39.37
Diesel	19.28	19.93	20.10
HCO	12.72	11.56	11.38
Coke	7.83	7.85	7.89
Yield of light oil	58.15	59.47	59.47
Yield of total oil	77.01	78.43	78.66
Conversion	67.68	68.25	68.33

ascribed to the introduction of intracrystalline mesopores via desilication. The introduced intracrystalline mesopores can improve the diffusivity and accessibility of ZSM-5.

When subsequent acid treatment is adopted, the FCC performance continues to be improved. The feedstock conversion is up to 68.33%, while the liquid petroleum gas yield is up to 19.19%. The reason for the improvement of sequential desilication–dealumination post treatment is that subsequent dealumination can remove the non-framework aluminum, unblock the micropore paths, thus increasing accessibility and restoring the micropore volume. It is crystal clear that in the preparation of the meso-ZSM-5 by desilication, removal of Al-rich debris by subsequent dealumination is essential. Increase of propylene yield from 5.67 to 6.11% for indicates the outstanding industrial application perspectives of sequential desilication–dealumination method in the near future.

4 Conclusions

In this work, meso-ZSM-5 zeolites were successfully prepared via sequential desilication–dealumination strategy. Desilication using NaOH proved to be effective for mesopore formation, which facilitates the connectivity between micropores. The subsequent dealumination

not only optimizes entire porosity through removing the Al-rich debris but also increases relative crystallinity and restores the acidity and Si/Al ratios. Catalytic performance in the FCC evaluation confirmed the superiority of sequential desilication–dealumination, which can be ascribed to the enhanced accessibility of the active sites situated inside the zeolite micropores. Moreover, the subsequent dealumination step carried out after desilication turns out to be indispensable, further promoting the activity of the meso-ZSM-5. Thus, sequential desilication–dealumination displays reliable advantages in the manufacture of hierarchical pore structure for ZSM-5 and implies its promising potential applications for constructing pore structure in other kinds of materials.

Acknowledgements This work was financially supported by the Petrochemical Joint Funds of NSFC-CNPC (Grant No. U1362202), Major Scientific and Technological Project of CNPC (Grant No. 2016E-0707), Fundamental Research Funds for the Central Universities (Grant No. 15CX05030A) and Innovation Project of China University of Petroleum (Grant No. YCX2015058).

References

1. C. Martínez, A. Corma, *Coord. Chem. Rev.* **255**, 1558 (2011)
2. A. Primo, H. Garcia, *Chem. Soc. Rev.* **43**, 7548 (2014)
3. F.J. Liu, T. Willhammar, L. Wang, L.F. Zhu, Q. Sun, X.J. Meng, W. Carrillo-Cabrera, X.D. Zou, F.S. Xiao, *J. Am. Chem. Soc.* **134**, 4557 (2012)
4. K. Möller, T. Bein, *Chem. Soc. Rev.* **42**, 3689 (2013)
5. D. Verboekend, T.C. Keller, S. Mitchell, J. Pérez-Ramírez, *Adv. Funct. Mater.* **23**, 1923 (2013)
6. M. Milina, S. Mitchell, P. Crivelli, D. Cooke, J. Pérez-Ramírez, *Nat. Commun.* (2014). doi:10.1038/ncomms4922
7. K. Egeblad, C.H. Christensen, M. Kustova, C.H. Christensen, *Chem. Mater.* **20**, 946 (2007)
8. T. Xue, C. Li, M. Wang, M. He, *Microporous Mesoporous Mater.* **156**, 97 (2012)
9. C.J. Jacobsen, C. Madsen, J. Houzvicka, I. Schmidt, A. Carlsson, *J. Am. Chem. Soc.* **122**, 7116 (2000)
10. Y.S. Tao, H. Kanoh, K. Kaneko, *J. Am. Chem. Soc.* **125**, 6044 (2003)
11. I. Schmidt, A. Boisen, E. Gustavsson, K. Ståhl, S. Pehrson, S. Dahl, A. Carlsson, C.J. Jacobsen, *Chem. Mater.* **13**, 4416 (2001)
12. F. Schmidt, C. Hoffmann, F. Giordanino, S. Bordiga, P. Simon, W. Carrillo-Cabrera, S. Kaskel, *J. Catal.* **307**, 238 (2013)
13. D. Wang, L. Xu, P. Wu, *J. Mater. Chem. A* **2**, 15535 (2014)
14. Z. Xue, T. Zhang, J. Ma, H. Miao, W. Fan, Y. Zhang, R. Li, *Microporous Mesoporous Mater.* **151**, 271 (2012)
15. R. Chal, C. Gerardin, M. Bulut, S.V. Donk, *ChemCatChem* **3**, 97 (2011)
16. M. Milina, S. Mitchell, N.L. Michels, J. Kenvin, J. Pérez-Ramírez, *J. Catal.* **308**, 398 (2013)
17. K.Y. Nandiwale, P.S. Niphadkar, S.S. Deshpande, V.V. Bokade, *J. Chem. Technol. Biotechnol.* **89**, 1507 (2014)
18. M. Ghavipour, R.M. Behbahani, G.R. Moradi, A. Soleimani-mehr, *Fuel* **113**, 310 (2013)
19. J.C. Groen, J.A. Moulijn, J. Pérez-Ramírez, *Ind. Eng. Chem. Res.* **46**, 4193 (2007)
20. X.W. Chang, L.F. He, H.N. Liang, X.M. Liu, Z.F. Yan, *Catal. Today* **158**, 198 (2010)
21. W. Schwieger, A.G. Machoke, T. Weissenberger, A. Inayat, T. Selvam, M. Klumpp, A. Inayat, *Chem. Soc. Rev.* (2016)
22. D. Verboekend, J. Pérez-Ramírez, *Catal. Sci. Technol.* **1**, 879 (2011)
23. M. Ogura, S.Y. Shinomiya, J. Tateno, Y. Nara, M. Nomura, E. Kikuchi, M. Matsukata, *Appl. Catal. A-Gen.* **219**, 33 (2001)
24. C. Fernandez, I. Stan, J.P. Gilson, K. Thomas, A. Vicente, A. Bonilla, J. Pérez-Ramírez, *Chem. Eur. J.* **16**, 6224 (2010)
25. M. Hartmann, *Angew. Chem. Int. Ed.* **43**, 5880 (2004)
26. M. Milina, S. Mitchell, Z.D. Trinidad, D. Verboekend, J. Pérez-Ramírez, *Catal. Sci. Technol.* **2**, 759 (2012)
27. Y.H. Kim, K.H. Lee, C.M. Nam, J.S. Lee, *ChemCatChem* **4**, 1143 (2012)
28. Z.T. Xue, T. Zhang, J.H. Ma, H.X. Miao, Y.Y. Zhang, R.F. Li, *Microporous Mesoporous Mater.* **151**, 271 (2012)
29. D. Verboekend, S. Mitchell, M. Milina, J.C. Groen, J. Pérez-Ramírez, *J. Phys. Chem. C* **115**, 14193 (2011)
30. J.C. Groen, W. Zhu, S. Brouwer, S.J. Huynink, F. Kapteijn, J.A. Moulijn, J. Pérez-Ramírez, *J. Am. Chem. Soc.* **129**, 355 (2007)
31. M. Milina, S. Mitchell, Z. Domínguez, *Catal. Mesoporous Sci. Technol.* **2**, 759 (2012)
32. P. Peng, Y.H. Wang, Z.Q. Zhang, K. Qiao, X.M. Liu, Z.F. Yan, F. Subhan, S. Komarneni, *Chem. Eng. J.* **302**, 323 (2016)
33. L. Zhao, C.M. Xu, S. Gao, B.J. Shen, *J. Mater. Sci.* **45**, 5406 (2010)
34. S. Brunauer, P.H. Emmett, E. Teller, *J. Am. Chem. Soc.* **60**, 309 (1938)
35. B. Lippens, J. De Boer, *J. Catal.* **4**, 319 (1965)
36. F. Thibault-Starzyk, I. Stan, S. Abelló, A. Bonilla, K. Thomas, C. Fernandez, J.P. Gilson, J. Pérez-Ramírez, *J. Catal.* **264**, 11 (2009)
37. J.M. Arandes, I. Torre, M.J. Azkoiti, J. Ereña, M. Olazar, J. Bilbao, *Energy Fuels* **23**, 4215 (2009)
38. C.S. Mei, P.Y. Wen, Z.C. Liu, H.X. Liu, Y.D. Wang, W.M. Yang, Z.K. Xie, W.M. Hua, Z. Gao, *J. Catal.* **258**, 243 (2008)
39. P. Peng, Y. Wang, M.J. Rood, Z. Zhang, F. Subhan, Z. Yan, L. Qin, Z. Zhang, Z. Zhang, X. Gao, *CrystEngComm* **17**, 3820 (2015)
40. J.C. Groen, J.A. Moulijn, J. Pérez-Ramírez, *Microporous Mesoporous Mater.* **87**, 153 (2005)